Journal of Inorganic and General Chemistry
ZAAC
Zeitschrift für anorganische und allgemeine Chemie
DOI: 10.1002/zaac.201900288
ARTICLE

Spin Interactions and Magnetic Anisotropy in a Triangular Nickel(II) Complex with Triaminoguanidine Ligand Framework

Michael Böhme,[a][‡] Dirk Schuch,[a][‡] Axel Buchholz,[a] Helmar Görls,[a] and Winfried Plass*[a]

Dedicated to Prof. Dr. Hans-Jörg Deiseroth on the Occasion of his 75th Birthday

Abstract. The trinuclear nickel(II) complex $[Ni_3(saltag^{rBu})(bpy)_3(H_2O)_3]Cl$ ($H_5saltag^{rBu}$ = 1,2,3-tris[(5-*tert*-butylsalicylidene)amino]guanidine) was synthesized and characterized by experimental as well as theoretical methods. The complex salt crystallizes with three molecules of dimethylformamide (dmf) and water as $[Ni_3(saltag^{rBu})(bpy)_3(H_2O)_3]Cl{\cdot}3dmf{\cdot}3H_2O$ (**1**) in the trigonal space group $P\bar{3}$, with the complex located on a threefold rotation axis, which is consistent with the molecular C_3 symmetry of the complex cation. Magnetic measurements reveal an antiferromagnetic coupling ($J = -35.9$ cm^{-1}) between the nickel(II) ions leading to a diamagnetic ground state for the trinuclear complex cation. Theoretical investigations based on broken-symmetry DFT confirm the antiferromagnetic exchange within the complex cation of **1**. Additional single-ion CASSCF ab initio studies reveal that magnetic anisotropy is present in the system. The experimental and theoretical results for **1** are compared with those of a structurally similar nickel(II) complex that is based on the bromo-substituted derivative of the triaminoguanidine ligand. The differences in their magnetic properties can be attributed to the stronger elongation of the pseudo-octahedral coordination sphere at the nickel(II) centers in case of **1**. The analysis of the magnetic properties of **1** clearly shows that for such exchange coupled systems reliable parameters for the magnetic anisotropy cannot be extracted from experimental data alone.

Introduction

Polynuclear transition-metal complexes continue to receive considerable attention because of their relevance to magnetically coupled active sites in metalloproteins and their potential applications as magnetic materials.[1] Polytopic ligands are part of the basic concept in supramolecular chemistry and crystal engineering.[2] In this context, threefold symmetric organic ligands constitute an interesting subgroup, due to their chemical versatility and the structural diversity of the resulting systems.[3] Symmetry is of particular interest to molecular magnetism, as the overlap of orbitals and thus the exchange interactions between the magnetic centers is crucially depended on symmetry.[4] Also in this case threefold symmetric systems are associated with favorable properties relevant to phenomena such as single-molecule magnets (SMMs)[5] and spin frustration.[6] The latter has been used to generate molecular electronic spin qubits based on trinuclear copper complexes.[7] Such triangular antiferromagnetic molecular systems are of particular interest due to possible spin-electric coupling effects, proposed as a promising mechanism for the control of molecular quantum systems,[8] for which recently experimental prove has been reported.[9]

However, tritopic ligands that induce strict C_3 symmetry in the resulting complex molecules are still rather scarce and to the best of our knowledge limited to ligands constituted from backbones based on triaminoguanidine[7,10] and phloroglucinol.[11] Interestingly, the triaminoguanidine core unit generally leads to antiferromagnetic exchange, whereas for copper(II) complexes with phloroglucinol-based ligands ferromagnetic exchange interactions via a spin-polarization mechanism are observed. Nevertheless, the *meta*-phenylene bridge in transition-metal complexes is not a general recipe for the construction of high-spin molecules, since in such systems opposing spin-delocalization and spin-polarization effects are operative.[12] On the other hand, the interplay of exchange coupling and magnetic anisotropy is of current interest for such triangular systems.[13]

In this work, we present the synthesis and characterization of the trinuclear nickel(II) complex based on the tritopic Schiff-base ligand 1,2,3-tris[(5-*tert*-butylsalicylidene)amino]guanidine ($H_5saltag^{rBu}$) depicted in Scheme 1. Its magnetic properties will be presented and analyzed on the basis of experimental results and theoretical methods, as the latter can provide a substantial benefit for understanding the magnetochemistry of complex magnetic systems.[14] A particular emphasis will be placed on the comparison with an earlier reported complex,[15] containing a ligand with electronically different substituents at the triaminoguanidine backbone.

Results and Discussion

Preparation

The tritopic ligand $H_5saltag^{rBu}$ (see Scheme 1) was synthesized via Schiff-base condensation of triaminoguanidine hy-

* Prof. Dr. W. Plass
Fax: +49 3641 948132
E-Mail: sekr.plass@uni-jena.de
[a] Institut für Anorganische und Analytische Chemie
Friedrich-Schiller-Universität Jena
Humboldtstraße 8
07743 Jena, Germany
[‡] These authors contributed equally to this article.
Supporting information for this article is available on the WWW under **http://dx.doi.org/10.1002/zaac.201900288** or from the author.

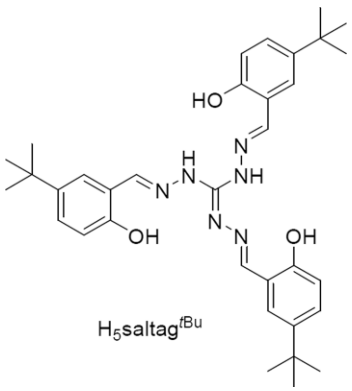

Scheme 1. Tritopic Schiff-base ligand 1,2,3-tris[(5-*tert*-butylsalicylidene)amino]guanidine ($H_5saltag^{tBu}$).

drochloride with 5-*tert*-butylsalicylaldehyde and subsequently isolated as monohydrochloride salt $H_5saltag^{tBu}$·HCl (for details see Experimental Section). The reaction of nickel(II) chloride hexahydrate with the hydrochloride salt of the ligand $H_5saltag^{tBu}$ in dimethylformamide (dmf) solution in the presence of 2,2'-bipyridine (bpy) as co-ligand and trimethylamine as base leads to the formation of the trinuclear nickel(II) complex that could be isolated as dark brown crystalline material. Characterization by elemental analysis, ESI mass spectrometry, IR spectroscopy, and X-ray crystallography revealed the presence of additional solvent molecules leading to the formula $[Ni_3(saltag^{tBu})(bpy)_3(H_2O)_3]Cl·3dmf·3H_2O$ (**1**).

The IR spectrum of the uncoordinated ligand shows a strong characteristic band at 1641 cm^{-1}, which can be attributed to ν(C=N) and ν(C=C) stretching vibrations of the conjugated system. Due to coordination of the nickel(II) cations in **1**, this band is shifted to 1598 cm^{-1}. Furthermore, the IR spectrum of **1** exhibits a broad band at 3249 cm^{-1}, indicating the presence of OH groups, and an additional sharp band at 1654 cm^{-1}, indicative for the presence of dmf molecules.

Structure Description

The trinuclear complex $[Ni_3(saltag^{tBu})(bpy)_3(H_2O)_3]Cl$ crystallizes in the trigonal space group $P\bar{3}$ (see Experimental Section for crystallographic details). The unit cell contains two symmetry-equivalent trinuclear nickel(II) complex cations, which are related by a center of inversion. In addition, three dmf as well as three water molecules co-crystallize together with each complex cation, resulting in the formation of a hydrogen network (see Figure S1, Supporting Information) including the chloride counterion, which is located on a special position (Wyckoff position 2d)[16] about 350 pm above the central carbon atom of the triaminoguanidine ligand. This network contains the threefold intramolecular Cl···HO hydrogen bonding between the chloride counterion and the apical water molecules at the central nickel(II) atoms (O1W···Cl1 315.5 pm), which is comparable in length to relevant cases with hydrogen bonds including nickel-bound chloride ligands.[17] The coordinated water molecules gives rise to additional hydrogen bonds to the oxygen atom of the neighboring co-crystallized dmf molecule (O1W···O1DA 275.6 pm). The hydrogen bonding network is completed by hydrogen bonds of the co-crystallized water molecule, which are connected to the nearby dmf molecule and the phenolate oxygen donor of the triaminoguanidine ligand (OW2···O1DA 306.4 pm, OW2···O1 280.8 pm). The different types of hydrogen bonds in the crystal structure of **1** are visualized in Figure S2 (Supporting Information).

The molecular structure of the complex cation $[Ni_3(saltag^{tBu})(bpy)_3(H_2O)_3]^+$ is depicted in Figure 1 together with the atom labeling of the first coordination sphere. The central carbon atom of the triaminoguanidine ligand is located on a special position (2d) leading to a molecular C_3 symmetry, with the three nickel(II) ions (Ni1) being crystallographically equivalent. The nickel(II) ion exhibits a pseudo-octahedral $[N_4O_2]$ coordination sphere, given by one of the tridentate pockets of the fully deprotonated tritopic Schiff-base ligand ($H_5saltag^{tBu}$), a 2,2′-bipyridine (bpy) co-ligand, and an additional water molecule. The latter being coordinated in one of the apical positions with respect to the tritopic Schiff-base ligand, whereas the bpy co-ligand provides an additional N donor atom (N3) in the equatorial plane formed together with the $[N_2O]$ donor set of the tritopic Schiff-base ligand (N1A, N2, and O1). The second N donor atom of the bpy co-ligand (N4) coordinates at the other apical position *trans* to the water ligand (O1W) at the Ni1 center.

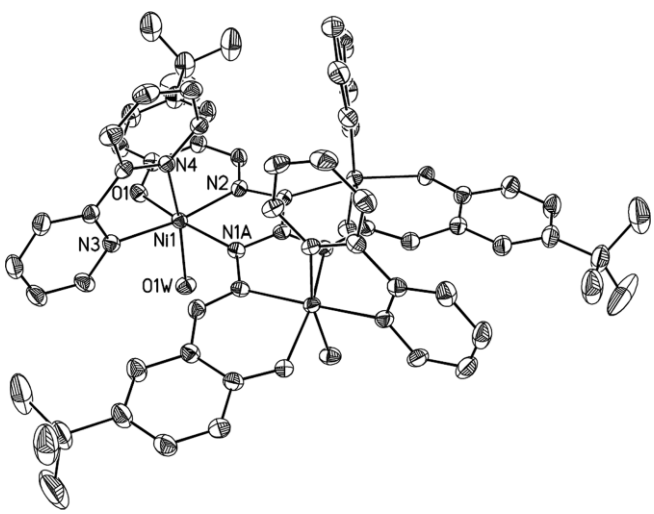

Figure 1. Molecular structure of the complex cation $[Ni_3(saltag^{tBu})(bpy)_3(H_2O)_3]^+$ together with the atom labeling of the first coordination sphere. Thermal ellipsoids are drawn at 50% probability level. Hydrogen atoms are omitted for clarity. Suffix A denotes symmetry equivalent atoms.

Continuous shape measures clearly show a deviation from an octahedral coordination sphere [$S(O_h)$ = 1.557; $S(O_h)$ = 0 refers to an ideal octahedron].[18] This is due, on the one hand, to a significant deviation of the bite angles related to the chelates given by the bpy co-ligand (N3–Ni–N4: 78.0°) and, on the other hand, on the triaminoguanidine ligand (N1A–Ni–N2: 77.9°, O1–Ni–N2: 90.7°). The distorted octahedral coordination polyhedra for the complex cation of **1** are visualized in Figure S3 (Supporting Information). Selected bond lengths and

angles for the first coordination sphere of the nickel(II) ion (Ni1) are listed in Table 1. In fact, a rather large range from 201.4 pm (Ni1–N2) to 214.6 pm (Ni1–O1W) is observed for the bond lengths at the Ni1 center, which again confirms the deviation from an ideal octahedral coordination sphere. Interestingly, a significant smaller variation of bond lengths, in the range from 201.9 pm (Ni1–N2) to 209.7 pm (Ni1–N3) is observed for the structurally related nickel(II) complex $[Ni_3(saltag^{Br})(bpy)_3(H_2O)_3]NO_3{\cdot}9H_2O{\cdot}1.5dmf$ (**2**) based on the bromo derivative of the triaminoguanidine ligand [$H_5saltag^{Br}$ = 1,2,3-tris[(5-bromosalicylidene)amino]guanidine].[15] Compound **2** crystallizes in the hexagonal space group $P6_3/m$ and likewise shows a molecular C_3 symmetry and extensive hydrogen bonding. Selected bond length and angles for the first coordination sphere of the nickel(II) center of **2** corresponding to those of **1** are included in Table 1.

Table 1. Selected bond lengths /pm) and angles /° for **1** (suffix A represents symmetry equivalent atoms created by the symmetry operation –y+1, x–y, z) together with corresponding bond parameters for **2**.[15]

	1	**2**
Ni1–O1	202.9(2)	203.7(3)
Ni1–O1W	214.6(2)	208.3(3)
Ni1–N1A	206.7(2)	208.4(3)
Ni1–N2	201.4(2)	201.9(3)
Ni1–N3	208.4(2)	209.7(3)
Ni1–N4	210.2(2)	209.4(4)
O1–Ni1–N1A	166.3(1)	167.13(13)
O1W–Ni1–N4	167.3(1)	168.71(13)
N2–Ni1–N3	171.1(1)	173.62(13)

From these data it becomes apparent that the bonds within the $[N_3O]$ equatorial coordination plane at the nickel(II) center (N1A, N2, N3, and O1) are generally somewhat shorter in the case of **1** compared to complex **2** with the bromo substituent, whereas the two axial bonds are elongated. Nevertheless, the electronic effect of a *para* substituent on a metal–phenolate bond length is typically rather small[19] and the observed Ni1–O1 bond is within the usual range.[20] However, it is interesting to note that the Ni1–N2 bond for both compounds is at the lower end of the usual range[21] and even slightly shorter than the corresponding Ni1–O1 bond. Consequently, rather than being attributed to the electronic effects, the geometric distortion and differences between the two compounds are most likely due to differences in the crystal packing related to the steric bulk of the *tert*-butyl group and the altered nature of the counterion (chloride and nitrate), both giving rise to variations in the hydrogen bonding network.

The most significant difference in the first coordination sphere of the two nickel(II) ions when the compounds **1** and **2** are compared is found in the bond lengths of the apical water ligand (**1**: 214.6 pm; **2**: 208.3 pm). This is accommodated by an overall axial elongation, which is somewhat compensated by more contracted bond lengths in the equatorial plane (Ni1–O1, Ni1–N1A, Ni1–N2, and Ni1–N3). Consequently, the nickel(II) center in compound **1** shows significantly larger distortion from an ideal octahedral coordination arrangement [$S(O_h)$ = 1.557] than observed for the substituted derivative **2** [$S(O_h)$ = 1.261].

Magnetic Measurements

The magnetochemistry of complex **1** was studied by dc magnetic susceptibility measurements in the temperature range between 2 and 300 K at a constant magnetic field of H_{dc} = 2000 Oe. The temperature dependence of the derived $\chi_M T$ data for complex **1** is presented in Figure 2. A room temperature value of about 2.84 $cm^3{\cdot}K{\cdot}mol^{-1}$ is observed for $\chi_M T$, which is close to the spin-only value expected for three independent nickel(II) ions (3.0 $cm^3{\cdot}K{\cdot}mol^{-1}$, for g = 2). Upon lowering the temperature, the $\chi_M T$ value decreases to nearly zero at very low temperatures indicative for a diamagnetic ground state (S = 0) for the trinuclear complex. This is consistent with the typically observed antiferromagnetic exchange interaction between paramagnetic centers mediated by N–N diazine bridges provided by the triaminoguanidine backbone of the ligand system.[7,13,15] In fact, antiferromagnetically exchange coupled trinuclear systems with equilateral triangular spin topology and individual centers of even spin such as nickel(II) ions (S = 1)[15,22] are well-known to possess a diamagnetic ground state.[23]

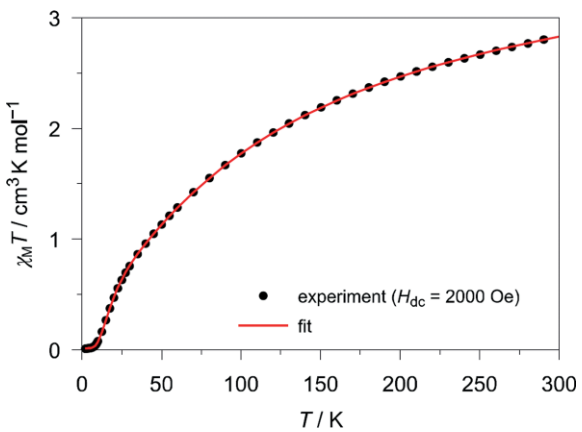

Figure 2. Temperature dependence of $\chi_M T$ for **1** depicted as black dots (●). The solid red line represents the best fit (see text).

The susceptibility data of **1** was fitted with the spin topology of an equilateral triangular arrangement (Figure S4, Supporting Information) based on the spin Hamiltonian given in equation (1) using the software package PHI.[24] Since the low temperature $\chi_M T$ value at 2 K still does not reach full zero (residual contribution of 0.01 $cm^3{\cdot}K{\cdot}mol^{-1}$), a correction for mononuclear impurities was included in the fit. Nevertheless, this paramagnetic impurity was found to be very small (ρ = 1.22 %). Furthermore, a correction term for temperature independent contributions χ_{tic} was included ($\chi_{tic} = 8.197 \times 10^{-4}$ $cm^3{\cdot}mol^{-1}$) [Equation (1)]:

$$\hat{H} = -J\left(\hat{S}_1\hat{S}_2 + \hat{S}_1\hat{S}_3 + \hat{S}_2\hat{S}_3\right) + g\mu_B\vec{H}\sum_{i=1}^{3}\hat{S}_i \quad (1)$$

The best fit obtained for the magnetic susceptibility data depicted in Figure 2 (red solid line) results to an antiferromagnetic exchange J = –35.9 cm^{-1} and confirms the diamagnetic ground state of **1**. The antiferromagnetic exchange in **1** is somewhat stronger than it was observed for **2** (J = –31.0 cm^{-1}),[15] which can be related to the shorter Ni–N bond lengths of the N–N

diazine moiety found in the complex cation of **1**. The obtained isotropic g value of 2.096 for **1** indicates a slight contribution from a second-order spin-orbit coupling leading to so-called magnetic anisotropy, since for the $^3A_{2g}[^3F]$ electronic ground state of a single nickel(II) ion the orbital momentum should be quenched ($L = 0$).

Magnetic anisotropy observed for nickel(II) ions can be included in the Hamiltonian, e.g., by an additional zero-field splitting (ZFS) term. A subsequent fit of the susceptibility data of **1** including a ZFS term for each of the nickel(II) centers led to an axial ZFS parameter of $D \approx 0$ ($S_{eff} = 1$). At this point, we have simulated the temperature dependence of $\chi_M T$ for **1** using the previously obtained best-fit parameters, but with inclusion of additional ZFS for each nickel(II) center. Figure 3 shows the simulated $\chi_M T$ curves for three different cases of the ZFS parameter $D = 0, \pm 15$ cm^{-1} in the temperature range 2–40 K (see Figure S5, Supporting Information, for the full temperature range 2–300 K). Interestingly, the effect of an additional ZFS term on the temperature dependence of $\chi_M T$ is rather small (Figure 3) and, as expected, not sensitive in sign.[23] In fact, this shows a significant correlation between the ZFS parameter D and the exchange coupling constant J, so that both can compensate each other without any significant influence on the fit of the $\chi_M T$ data. Moreover, the diamagnetic ground state of complex **1** ($S = 0$) is not affected by single-ion magnetic anisotropy. As a matter of fact, for this class of antiferromagnetically exchange coupled systems a ZFS term cannot be obtained by fitting the susceptibility data.

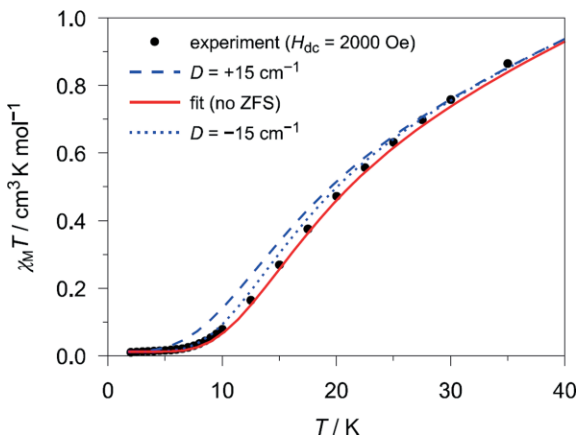

Figure 3. Temperature dependence of $\chi_M T$ for **1**: experimental data (●) and fit without ZFS ($D = 0$; solid red line) The blue lines represent simulations utilizing the best-fit parameters (see text) together with an arbitrary ZFS of either easy-axis ($D < 0$; blue dotted line) or easy-plane type of magnetic anisotropy ($D > 0$; blue dashed line).

Computational Studies

For the complex cations of compounds **1** and **2** computational studies have been performed to gain further insight into their magnetic properties with a particular emphasis on the influence of geometric distortion on properties such as magnetic exchange and anisotropy. Of additional interest are possible electronic effects introduced through the *para* substituents (*tert*-butyl or bromo) at the salicylidene moiety of the triaminoguanidine ligand. In this context, we also investigated the electronic properties of the two fully deprotonated anions of the tritopic ligand systems H_5saltag^{Br} and H_5saltag^{tBu}, which might influence their coordination properties with respect to the nickel(II) ions. The corresponding structures have been optimized at the DFT level of theory retaining the C_{3h} symmetry of the ligand system (see Figure S6, Supporting Information). A comparison of the charges of the donor atoms derived from natural population analysis[25] (NPA) shows that the influence of the *para* substituent is nearly negligible, with the largest difference between corresponding charges of the donor atoms of both ligands being 0.005. This, like the observed behavior of the bond lengths (vide supra), suggests that only minor contributions from electronic ligands effects influence the differences of the magnetic properties of compounds **1** and **2**.

Magnetic Exchange Interactions

The magnetic exchange interactions present in the complex cations of compounds **1** and **2** were studied by broken-symmetry DFT (BS-DFT) calculations utilizing the B3-LYP hybrid functional, which was previously found to give reasonable results for magnetic exchange coupling constants in 3d transition metal complexes[26] and in particular for cases of triangular systems.[7,13,27] For these calculations, two different approaches have been used: (i) Evaluation of the exchange coupling constant from a dinuclear model structure generated by diamagnetic substitution of one paramagnetic nickel(II) center with a zink(II) ion, namely $[Ni_2Zn(saltag^{tBu})(bpy)_3(H_2O)_3]^+$, further denoted as **1-Ni$_2$Zn**. (ii) Mapping the energy difference between the high-spin (HS) and broken-symmetry (BS) state onto the pairwise interactions of the paramagnetic nickel(II) centers utilizing the full structure $[Ni_3(saltag^{tBu})(bpy)_3(H_2O)_3]^+$, further referred to as **1-Ni$_3$** (see Figure S7, Supporting Information). For both model structures, the coordinates of all non-hydrogen atoms were taken from the crystal structure of **1**, whereas the positions of the hydrogen atoms were energy optimized. Assuming that the non-spin-projected energies derived for the corresponding HS and BS states can be used for the evaluation of the exchange coupling constant in both approaches (cf. Table S1, Supporting Information),[28] (i) **1-Ni$_2$Zn** leads to $J = -32.9$ cm^{-1} ($\Delta E = E_{BS} - E_{HS} = 3J$) and (ii) **1-Ni$_3$** leads to $J = -35.1$ cm^{-1} ($\Delta E = E_{BS} - E_{HS} = 6J$). Both values are in good agreement with the exchange coupling constant $J = -35.9$ cm^{-1} derived from the experimental data.

The corresponding spin-density plots for the HS and BS states show only a slight delocalization of the spin density onto the bridging ligand backbone (see Figures S8 and S9, Supporting Information). In case of the all-nickel structural model **1-Ni$_3$** NPA for the HS state reveals a slightly higher spin polarization at donor atom N2 (0.067) as compared to the phenolate donor atom O1 (0.060) which is in agreement with the shorter Ni–N2 bond length as compared to the Ni–O1 bond. Moreover, it is evident that the magnetic exchange is primarily mediated by the N–N diazine bridges of the triaminoguanidine moiety, since only a rather small spin density is found at the central

carbon atom C1, which is located at the C_3 rotational axis [**1-Ni$_3$**: –0.008 (HS); –0.018 (BS)].

Analogous BS-DFT calculations were performed for model structures of compound **2**, i.e., $[Ni_3(saltag^{Br})(bpy)_3(H_2O)_3]^+$ (**2-Ni$_3$**) and $[Ni_2Zn(saltag^{Br})(bpy)_3(H_2O)_3]^+$ (**2-Ni$_2$Zn**) (see Figure S10, Supporting Information). In case of **2**, a slightly weaker antiferromagnetic exchange is obtained (**2-Ni$_3$**: –32.2 cm^{-1}; **2-Ni$_2$Zn**: –30.7 cm^{-1}; see also Table S2, Supporting Information), which is in excellent agreement with the reported experimental value for the exchange coupling constant J = –31.0 cm^{-1}.[15] In fact, this also reproduces the trend observed for the experimental J values, which indicates a slight decrease in the coupling strength when the *tert*-butyl derivative **1** is compared with the bromo derivative **2**. Spin density plots obtained for the structural models **2-Ni$_3$** and **2-Ni$_2$Zn** show a high similarity in terms of delocalization of the spin density with those observed for the corresponding models of **1** (see Figures S11 and S12, Supporting Information).

Single-Ion Magnetic Anisotropy

High-level single-ion ab initio multi-reference calculations have been performed to gain insight into the single-ion magnetic anisotropy of the nickel(II) centers of the complex cations of compounds **1** and **2**, which have not been possible on the basis of the experimental magnetic susceptibility data (see also Computational Details). In order to keep the computational effort feasible in these theoretical studies, simplified structural models were used in which two of the paramagnetic nickel(II) centers are replaced by diamagnetic zink(II) ions, further referred to as **1-Ni1** and **2-Ni1** for **1** and **2**, respectively (see Figure S13, Supporting Information). The relative CASSCF energies reveal a high-spin $^3A_{2g}[^3F]$ ground state for the nickel(II) centers in **1** and **2** (see Table S3, Supporting Information), as excepted for nickel(II) ions in a (pseudo-)octahedral coordination arrangement. It should be noted, however, that this high-spin state (S = 1) for a single nickel(II) ion does not represent the diamagnetic molecular ground state (S = 0), since the single-ion ab initio calculations neglect the magnetic exchange between the paramagnetic centers. Nevertheless, the single-ion data provides valuable information about the single-ion magnetic anisotropy, which can serve as a basis for the simulation of the trinuclear molecular system (vide infra). The calculations for the single ions further show that the lowest singlet state, which is the anticipated ground state multiplet for nickel(II) ions in a square-planar coordination environment, is well-separated from the ground state (**1-Ni1**: 17430 cm^{-1}; **2-Ni1**: 17943 cm^{-1}, cf. Table S3, Supporting Information). The $^3A_{2g}[^3F]$ ground multiplet itself consists of three low-lying spin-orbit coupled states [$(2S + 1)\times(2L + 1)$ = 3] that are non-degenerate, which is due to the fact that nickel(II) is a non-Kramers ion. The corresponding energies observed for **1-Ni1** and **2-Ni1** (see Table S4, Supporting Information) reveal a larger energy splitting range in case of **1-Ni1** (**1-Ni1**: 14.5 cm^{-1}; **2-Ni1**: 10.8 cm^{-1}), which is consistent with its more pronounced axial elongation (vide supra).

The energetic splitting of the $^3A_{2g}[^3F]$ ground multiplet in **1-Ni1** and **2-Ni1** can be described in terms of an effective ZFS Hamiltonian (S_{eff} = 1). A negative axial ZFS parameter D is obtained in both cases (**1-Ni1**: –11.5 cm^{-1}, **2-Ni1**: –9.0 cm^{-1}), indicating an easy-axis type of magnetic anisotropy ($D < 0$). In addition, a strong rhombic distortion of the magnetic anisotropy is evident from a non-zero rhombic ZFS parameter E (**1-Ni1**: –3.0 cm^{-1}, **2-Ni1**: –1.8 cm^{-1}), leading to a significant $|E/D|$ ratio (**1-Ni1**: 0.26; **2-Ni1**: 0.20) for the nickel(II) centers of both compounds. These values are well within the range typical observed for octahedral nickel(II) complexes.[29] Figure 4 shows the magnetic anisotropy axes obtained for a single-ion of **1-Ni1** (for **2-Ni1** cf. Figure S14, Supporting Information). The orientation of the single-ion easy axis is primarily determined by the binding vector of the shortest bond (Ni1–N2, cf. Table 1) within the coordination polyhedron, with a tilting angle of 11.3° and 13.0° for **1-Ni1** and **2-Ni1**, respectively. It should be noted at this point that the presence of the short Ni1–N2 bond within the octahedral coordination sphere of the nickel(II) centers in **1** and **2** is directly related to the rather weak axial coordination of a neutral water (Ni1–O1W) and bpy ligand (Ni1–N4). The latter leads to an axial elongation at the nickel(II) centers, which is more pronounced in the case of **1** (vide supra).

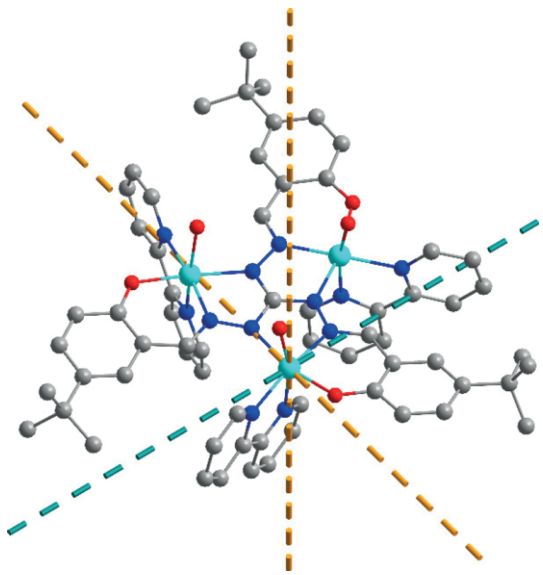

Figure 4. Anisotropy axes (teal dashed line: easy axis; orange dashed lines: hard plane) obtained from single-ion ab initio multi-reference calculations for the $^3A_{2g}[^3F]$ ground state and projected on the cationic complex molecule of **1**. Hydrogen atoms are omitted for clarity.

The magnetic anisotropy for the individual nickel(II) centers in both compounds, i.e., **1-Ni1** and **2-Ni1**, can also be described by the Cartesian components of the g factor of the $^3A_{2g}[^3F]$ ground multiplet (Table S5, Supporting Information), which again show significant rhombic distortion ($g_x \neq g_y \neq g_z$). Their relative orientation within the molecular framework is depicted in Figures S15 and S16 (Supporting Information). From this data it is obvious that the easy axis of magnetization g_z coincides with the easy axis of the ZFS Hamiltonian. The somewhat shorter Ni1–N2 bond in **1** leads to a slightly larger g_z value in case of **1-Ni1** (**1-Ni1**: 2.310; **2-Ni1**: 2.292). At the same time, the elongation of the axial Ni1–O1W bond in **1**

with respect to **2** results in a decrease of the corresponding g_x value for **1-Ni1** (**1-Ni1**: 2.208; **2-Ni1**: 2.217). As a result, the magnetic anisotropy in terms of Cartesian g factors expressed by $\Delta = (g_z - g_x)$ is larger in **1-Ni1** (0.102) as compared to **2-Ni1** (0.075).

Anisotropic Exchange-Coupled Trinuclear System

The magnetic behavior of the antiferromagnetically coupled trinuclear nickel(II) complex cation of **1** can be described on the basis of the single-ion ab initio multi-reference calculations presented above utilizing the POLY_ANISO program. Although this allows to link theoretical and experimental magnetic data, from the side of theory the exchange coupling constant is still a critical issue, since this parameter cannot be determined on the basis of high-level ab initio methods. At present, there are two ways to overcome this case, by either using the values derived from BS-DFT calculations or by fitting the exchange coupling constant based on the single-ion ab initio results to the experimental susceptibility data (see Computational Details).[14d] The fitting approach leads to an exchange coupling constant of $J = -43.1$ cm^{-1} for **1-Ni1**, which is somewhat larger than the parameter derived from BS-DFT calculations (**1-Ni$_3$**: –35.1 cm^{-1}; **1-Ni$_2$Zn**: –32.9 cm^{-1}), but is still in acceptably agreement with the experimental value of $J = -35.9$ cm^{-1}. The simulated magnetic susceptibility based on the single-ion magnetic anisotropy data of the structural model **1-Ni1** is shown in Figure S17 (Supporting Information) for the temperature range 2–100 K.

The energy spectrum of spin states for the trinuclear systems with and without inclusion of magnetic anisotropy is depicted in Figure 5 with a scaling based on the magnetic coupling constant J. Here, the scale given for the isotropic Heisenberg system corresponds to the Hamiltonian used to fit the experimental susceptibility data, while for **1** and **2** the magnetic anisotropy data derived for the structural models **1-Ni1** and **2-Ni1** were used for the simulations. For the case of an ideal isotropic Heisenberg system, all microstates belonging to the same $(2S + 1)$-fold spin multiplet are degenerate. Whereas additionally taking into account the magnetic anisotropy leads to a lifting of the degeneracy for the microstates. In fact, the observed broadening of the spin multiplets in the case of **1** is more pronounced than for complex **2**, which is a result of the higher magnetic anisotropy based on the geometrical distortions observed in **1** (vide supra).

Conclusions

This work presents the synthesis and characterization of the triangular nickel(II) complex **1** derived from a *tert*-butyl-substituted tritopic triaminoguanidine ligand system. The trinuclear complex cation exhibits a crystallographically imposed molecular C_3 symmetry with identical nickel(II) ions, for which the coordination is saturated by an additional 2,2′-bipyridine and water co-ligand. The distorted octahedral coordination sphere of the nickel(II) centers in **1** shows an axial elongation along the axis given by the oxygen donor of the water

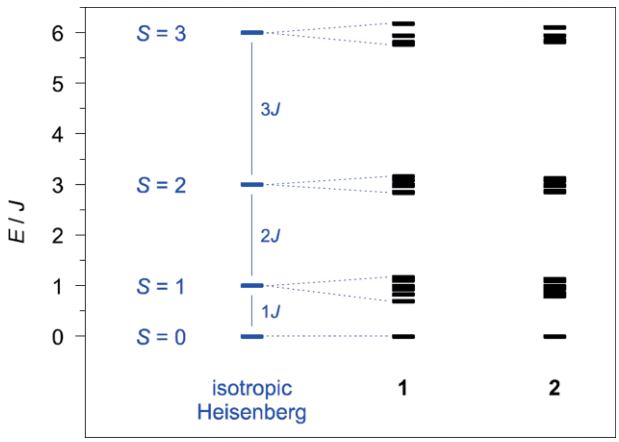

Figure 5. Energy spectrum of spin states for the isotropic Heisenberg case of an antiferromagnetically coupled ($J < 0$) triangular nickel(II) system (blue). The spectra given for **1** and **2** are obtained by simulations with POLY_ANISO utilizing the magnetic anisotropy data from single-ion ab initio calculations of the structural models **1-Ni1** and **2-Ni1**.

ligand and one of the nitrogen donors of the 2,2′-bipyridine co-ligand. The N–N diazine bridges of the triaminoguanidine moiety give rise to antiferromagnetic exchange interactions between the nickel(II) centers of the trinuclear complex cation. The experimental exchange coupling constant of –35.9 cm^{-1} is in good agreement with the values derived from BS-DFT calculations. It is important to note, that it is not possible to derive any reliable information on the magnetic anisotropy from the experimental susceptibility data, as the fit of the low-temperature data for such an exchange coupled system is insensitive toward inclusion of a ZFS parameter in the Hamiltonian. However, high-level ab initio multi-reference calculations for single-ion fragments based on the trinuclear molecular structure show that the pseudo-octahedral nickel(II) coordination sphere leads to a significant magnetic anisotropy with an easy axis ($D = -11.5$ cm^{-1}) paired with a strong rhombic distortion ($E = -3.0$ cm^{-1}). This magnetic anisotropy results in the lifting of the degeneracy of the excited spin multiplets. This effect is less pronounced for the analogous bromo derivative, which can be attributed to the smaller geometric distortions in this case.

Experimental Section

Materials and Physical Measurements: Triaminoguanidine hydrochloride was prepared according to literature.[30] All other chemicals and solvents are commercially available and were used as received without further purification. IR spectra for samples prepared as KBr pellets were measured on a Bruker IFS55/Equinox spectrometer with a Raman unit FRA 106/S. In addition, a Specac Golden Gate ATR unit was used for measurements on pure samples. NMR experiments (^{1}H, ^{13}C) were carried out on a Bruker AVANCE 400 spectrometer. The chemical shifts were referenced to tetramethylsilane. Elemental analyses (C, H, N) were acquired by use of a Leco CHNS-932 elemental analyzer. Mass spectra were measured on a MAT 95XL Finnigan instrument for electrospray ionization (ESI).

Synthesis of H_5saltag^{rBu}·HCl: A solution of 5-*tert*-butylsalicylaldehyde (2.2 g, 12.3 mmol) in methanol (20 mL) was added dropwise to a stirred solution of triaminoguanidine hydrochloride (0.579 g, 4.1 mmol) in water (3 mL). The resulting reaction mixture was refluxed overnight followed by evaporation of the solvent. The resulting yellow solid was dried in vacuo. Yield: 0.25 g (66 %). **^{1}H NMR** ([D$_6$]DMSO, ppm): δ = 12.13 (s, 3 H, NH), 10.18 (s, 3 H, OH), 9.02 (s, 3 H, HC=N), 8.00 (s, 3 H, H_{ph}), 7.38 (d, ^3J = 8 Hz, 3 H, H_{ph}), 6.96 (d, ^3J = 8 Hz, 3 H, H_{ph}), 1.33 (s, 27 H, CH_3). **^{13}C NMR** ([D$_6$]DMSO, ppm): δ = 155.6, 149.2, 142.1, 130.1, 123.9, 119.0, 116.5, 34.4 ($C(CH_3)_3$), 31.8 (CH_3). **IR** (KBr): $\tilde{\nu}$ = 3391 (br, OH), 2961 (s, CH_3 ν_{as}), 2869 (m, CH_3 ν_s), 1641 (vs, br, C=N and C=C), 1462 (w), 1423 (w), 1394 (w), 1363 (m), 1335 (m), 1242 (m), 1185 (m), 962 (w), 829 (w), 740 (w) cm^{-1}. **MS** (Micro-ESI positive mode in $CHCl_3$ + MeOH): *m/z* (%) = 745.3 (10), 585.4 (100) (H_6saltag^{rBu})$^+$. EA for H_6saltag^{rBu}Cl·1/3CH_3OH ($C_{34.3}H_{46.3}ClN_6O_{3.3}$, M = 631.9 g·mol^{-1}): calcd: C 65.26, H 7.39, N 13.30 %; found: C 65.65, H 7.76, N 12.89 %.

Synthesis of [Ni$_3$(saltag^{rBu})(bpy)$_3$(H$_2$O)$_3$]Cl·3dmf·3H$_2$O (1): To a stirred green solution of $NiCl_2$·6 H_2O (225.3 mg, 0.95 mmol) and H_6saltag^{rBu}Cl (0.32 mmol) in dimethylformamide (5 mL) was added a solution of triethylamine (191 mg, 1.9 mmol) in methanol (5 mL). To the brownish suspension a solution of 2,2'-bipyridine (148 mg, 0.95 mmol) in methanol (5 mL) was added. The resulting dark brownish-red solution was stirred at ambient temperature for further 5 min followed by filtration. Within several days dark brown crystals were formed which were collected by filtration and dried in air. Yield: 0.360 g (74 %). **IR** (ATR): $\tilde{\nu}$ = 3249 (w, br (OH)), 2950 (m, CH_3 ν_{as}), 2900 (vw, CH_3 ν_s), 2866 (vw, CH_3 ν_s), 1654 (s), 1598 (m), 1532 (w, br), 1483 (s, C=N and C=C), 1441 (vs), 1388 (m), 1355 (s), 1316 (m), 1255 (m), 1207 (w, br), 1181 (s), 1125 (s), 1058 (w), 1043 (vw), 1023 (w), 923 (w), 818 (m), 768 (s), 737 (m), 696 (m), 664 (m), 651 (w), 630 (w), 615 (w), 571 (m), 523 (m), 479 (m), 456 (m) cm^{-1}. **MS** (Micro-ESI positive mode in CH_3OH): *m/z* (%) = 1222.8 (100) [Ni$_3$(saltag^{rBu})(bpy)$_3$]$^+$, 1099.8 (20) [Ni$_3$(saltag^{rBu})(bpy)$_2$(CH_3OH)]$^+$, 1067.3 (60) [Ni$_3$(saltag^{rBu})(bpy)$_2$]$^+$, 988.8 (20). EA for [Ni$_3$(saltag^{rBu})(bpy)$_3$(H$_2$O)$_3$]Cl·3dmf·3H$_2$O ($C_{73}H_{96}ClN_{15}Ni_3O_{12}$, M = 1587.22 g·mol^{-1}): calcd. C: 55.22, H: 6.10, N: 13.24 %; found: C: 54.90, H: 5.82, N: 13.09 %.

X-ray Crystallography: Crystals of complex **1** suitable for X-ray crystallography were obtained directly from the mother liquor. The crystallographic data were collected on a Nonius Kappa CCD diffractometer at 133 K using graphite-monochromated Mo-K_α radiation (71.073 pm). Data were corrected for Lorentz as well as polarization effects[31] and absorption was taken into account on a semi-empirical basis using multiple-scans (SADABS 2016/2).[32] The structure was solved by direct methods (SHELXS) and refined by full-matrix least-squares techniques against F^2 (SHELXL-2018).[33] The hydrogen atom bonded to water molecules O1W and O2W were located by difference Fourier synthesis and refined isotropically. All other hydrogen atoms were included at calculated positions with fixed thermal parameters. All non-hydrogen atoms were refined anisotropically. A summary of crystallographic and structure refinement data is given in Table 2.

Crystallographic data (excluding structure factors) for the structure in this paper have been deposited with the Cambridge Crystallographic Data Centre, CCDC, 12 Union Road, Cambridge CB21EZ, UK. Copies of the data can be obtained free of charge on quoting the depository number CCDC-1962909 for structure **1** (Fax: +44-1223-336-033; E-Mail: deposit@ccdc.cam.ac.uk, http://www.ccdc.cam.ac.uk)

Magnetic Measurements: Magnetic susceptibility data were obtained from powdered samples in gelatin capsules using a Quantum-Design MPMS-5 SQUID magnetometer equipped with a 5 T magnet in the range from 2 to 300 K. The measured data were corrected for diamagnetism of the capsules and the intrinsic diamagnetism of the sample, estimated by measurements on a similar ligand system. The molar susceptibility data of the complexes is based on the molecular weights calculated from the elemental analyses data. Fitting of the dc SQUID data was done using least-squares full-matrix diagonalization approach as implemented in the PHI program and the spin Hamiltonian as given in Equation (1).

Table 2. Crystallographic data for [Ni$_3$(saltag^{rBu})(bpy)$_3$(H$_2$O)$_3$]Cl·3dmf·3H$_2$O (**1**).

	1
Empirical formula	$C_{73}H_{96}ClN_{15}Ni_3O_{12}$
Formula weight /g·mol^{-1}	1587.22
Crystal system	trigonal
Space group	$P\bar{3}$ (no. 147)
a /pm	2056.02(3)
b /pm	2056.02(3)
c /pm	1079.39(2)
α /°	90.0
β /°	90.0
δ /°	120.0
V /nm^3	3.95151(14)
Temperature /°C	–140
Z	2
μ(Mo-K_α) /mm^{-1}	0.808
θ range of data collection /°	2.74 ≤ θ ≤ 27.48
Measured reflections	23868
Unique reflections	6025
R_{int}	0.0438
Goodness-of-fit on F^2	1.069
Final *R* indices [all data]	R_1 = 0.0605, wR_2 = 0.1046
Final *R* indices [$I > 2\sigma(I)$]	R_1 = 0.0464, wR_2 = 0.0972

Computational Details: Structural models for the theoretical studies are based on the atomic positions of the single-crystal structure of **1**, with the positions of all hydrogen atoms optimized with the Turbomole 7.2 package of programs[34] at RI-DFT-D3[35]/BP86[36]/def2-SVP[37] level of theory. Within these optimizations all nickel(II) ions were replaced by diamagnetic zinc(II) ions to reduce the computational effort. Broken-symmetry density functional theory (BS-DFT) calculations were performed to investigate intramolecular magnetic coupling on the basis of a cationic trinuclear nickel(II) complex [Ni$_3$(saltag^{rBu})(bpy)$_3$(H$_2$O)$_3$]$^+$. These calculations were performed utilizing the B3-LYP hybrid functional[38] in combination with the def2-TZVPP basis sets[37] and tight self-consistent field (SCF) convergence criteria (1×10^{-8} Hartree). The magnetic coupling constant *J* was calculated for an isotropic Heisenberg Hamiltonian ($\hat{H} = -J\ \hat{S}_1\ \hat{S}_2$).Analogous BS-DFT calculations at the same level of theory have been performed for the trinuclear complex cation of a literature-known compound, namely [Ni$_3$(saltag^{Br})(bpy)$_3$(H$_2$O)$_3$]$^+$.

Single-ion properties were studied by multi-reference ab initio calculations performed with the OpenMolcas package of programs in version 18.09.[39] To reduce the computational effort these calculations are based on a structurally simplified model of the complex cation of **1**, which is visualized in Figure S13 (Supporting Information). The complete active space self-consistent field (CASSCF) approach was used with 8 electrons in 10 orbitals (3d and 4d shell) to adequately take the so-called 'double d-shell' effect into account.[40] State-average CASSCF calculations for two multiplicities with a different number of roots have been calculated: 10 roots for $2S + 1 = 3$ and 15 roots for $2S + 1 = 1$. Scalar-relativistic effects were treated by a second-order

Douglas–Kroll–Hess Hamiltonian combined with ANO-RCC basis sets (for basis set details see Table S6, Supporting Information).[41] Subsequently, spin–orbit coupling interactions, which allow a mixing of states of different multiplicities, were included by the RASSI-SO program. Magnetic properties such as *g* factors and zero-field splitting (ZFS) parameters for a single nickel(II) ion have been obtained by the SINGLE_ANISO module. The trinuclear cationic complex system was simulated with the POLY_ANISO program on the basis of the data from ab initio calculations.[42] For this simulation a coupling constant was employed which was determined by minimizing the residual between the experimental and theoretical $\chi_M T$ product in a temperature range of 2–100 K.

Supporting Information (see footnote on the first page of this article): Representation of hydrogen bonds and coordination polyhedra, spin coupling scheme, DFT ligand studies, BS-DFT computational models and results, ab initio computational models and results.

Keywords: Triaminoguanidine; Nickel; Quantum chemistry; Magnetochemistry; Magnetic anisotropy

References

[1] a) D. Gatteschi, R. Sessoli, J. Villain, *Molecular Nanomagnets*, Oxford University Press, Oxford, **2006**; b) *Magnetism: Molecules to Materials, Vol. I–V* (Eds.: J. S. Miller, M. Drillon), Wiley-VCH, Weinheim, **2001–2005**; c) W. Plass, *Chem. Unserer Zeit* **1998**, *32*, 323–333; d) R. H. Holm, P. Kennepohl, E. I. Solomon, *Chem. Rev.* **1996**, *96*, 2239–2314.

[2] a) K. K. Gangu, S. Maddila, S. B. Mukkamala, S. B. Jonnalagadda, *Inorg. Chim. Acta* **2016**, *446*, 61–74; b) T.-H. Chen, I. Popov, W. Kaveevivitchai, O. Š. Miljanić, *Chem. Mater.* **2014**, *26*, 4322–4325; c) S. Kitagawa, R. Kitaura, S. Noro, *Angew. Chem. Int. Ed.* **2004**, *43*, 2334–2375; d) B. Moulton, M. J. Zaworotko, *Chem. Rev.* **2001**, *101*, 1629–1658.

[3] a) W. J. Su, L. C. Liang, *Inorg. Chem.* **2018**, *57*, 553–556; b) I. Kisets, D. Gelman, *Organometallics* **2018**, *37*, 526–529; c) O. Akintola, D. Hornig, A. Buchholz, H. Görls, W. Plass, *Dalton Trans.* **2017**, *46*, 8037–8050; d) O. Akintola, S. Ziegenbalg, A. Buchholz, H. Görls, W. Plass, *CrystEngComm* **2017**, *19*, 2723–2732; e) C. Segarra, J. Linke, E. Mas-Marza, D. Kuck, E. Peris, *Chem. Commun.* **2013**, *49*, 10572–10574; f) Y. Liu, W. Xuan, H. Zhang, Y. Cui, *Inorg. Chem.* **2009**, *48*, 10018–10023; g) P. J. Lusby, P. Müller, S. J. Pike, A. M. Z. Slawin, *J. Am. Chem. Soc.* **2009**, *131*, 16398–16400; h) M. J. Prushan, N. K. Privette, M. Zeller, A. D. Hunter, S. Lofland, S. D. Preite, *Inorg. Chem. Commun.* **2007**, *10*, 631–635; i) A. Zharkouskaya, A. Buchholz, W. Plass, *Eur. J. Inorg. Chem.* **2005**, *2005*, 4875–4879; j) A. Zharkouskaya, H. Görls, G. Vaughan, W. Plass, *Inorg. Chem. Commun.* **2005**, *8*, 1145–1148; k) M. Pascu, F. Lloret, N. Avarvari, M. Julve, M. Andruh, *Inorg. Chem.* **2004**, *43*, 189–519; l) J. Leveque, C. Moucheron, A. Kirsch-De Mesmaeker, F. Loiseau, S. Serroni, F. Puntoriero, S. Campagna, H. Nierengarten, A. Van Dorsselaer, *Chem. Commun.* **2004**, 878–879; m) B. Conerney, P. Jensen, P. E. Kruger, C. MacGloinn, *Chem. Commun.* **2003**, 1274–1275; n) M. V. Ovchinnikov, B. J. Holliday, C. A. Mirkin, L. N. Zakharov, A. L. Rheingold, *Proc. Natl. Acad. Sci. USA* **2002**, *99*, 4927–4931.

[4] H. Weihe, H. U. Güdel, *Inorg. Chem.* **1997**, *36*, 3632–3639.

[5] T. Glaser, M. Heidemeier, T. Weyhermüller, R. D. Hoffmann, H. Rupp, P. Müller, *Angew. Chem. Int. Ed.* **2006**, *45*, 6033–6037.

[6] a) J. Schnack, *Dalton Trans.* **2010**, *39*, 4677–4686; b) M. L. Baker, G. A. Timco, S. Piligkos, J. S. Mathieson, H. Mutka, F. Tuna, P. Kozlowski, M. Antkowiak, T. Guidi, T. Gupta, H. Rath, R. J. Woolfson, G. Kamieniarz, R. G. Pritchard, H. Weihe, L. Cronin, G. Rajaraman, D. Collison, E. J. McInnes, R. E. Winpenny, *Proc. Natl. Acad. Sci. USA* **2012**, *109*, 19113–19118.

[7] a) E. T. Spielberg, A. Gilb, D. Plaul, D. Geibig, D. Hornig, D. Schuch, A. Buchholz, A. Ardavan, W. Plass, *Inorg. Chem.* **2015**, *54*, 3432–3438; b) B. Kintzel, M. Böhme, J. Liu, A. Burkhardt, J. Mrozek, A. Buchholz, A. Ardavan, W. Plass, *Chem. Commun.* **2018**, *54*, 12934–12937.

[8] a) M. Trif, F. Troiani, D. Stepanenko, D. Loss, *Phys. Rev. Lett.* **2008**, *101*, 217201; b) M. Trif, F. Troiani, D. Stepanenko, D. Loss, *Phys. Rev. B* **2010**, *82*, 045429.

[9] a) J. Liu, J. Mrozek, W. K. Myers, G. A. Timco, R. E. P. Winpenny, B. Kintzel, W. Plass, A. Ardavan, *Phys. Rev. Lett.* **2019**, *122*, 037202; b) M. Fittipaldi, A. Cini, G. Annino, A. Vindigni, A. Caneschi, R. Sessoli, *Nat. Mater.* **2019**, *18*, 329–334; c) A. K. Boudalis, J. Robert, P. Turek, *Chem. Eur. J.* **2018**, *24*, 14896–14900.

[10] W. Plass, *Coord. Chem. Rev.* **2009**, *253*, 2286–2295.

[11] a) T. Glaser, H. Theil, M. Heidemeier, *C. R. Chim.* **2008**, *11*, 1121–1136; b) E. T. Spielberg, W. Plass, *Eur. J. Inorg. Chem.* **2010**, *2010*, 3093–3096; c) D. Plaul, W. Plass, *Inorg. Chim. Acta* **2011**, *374*, 341–349; d) T. Glaser, *Coord. Chem. Rev.* **2013**, *257*, 140–152; e) J. Oldengott, A. Stammler, H. Bögge, T. Glaser, *Dalton Trans.* **2015**, *44*, 9732–9735.

[12] D. Plaul, A. Buchholz, H. Görls, W. Plass, *Polyhedron* **2007**, *26*, 4581–4590.

[13] D. Plaul, M. Böhme, S. Ostrovsky, Z. Tomkowicz, H. Görls, W. Haase, W. Plass, *Inorg. Chem.* **2018**, *57*, 106–119.

[14] a) L. F. Chibotaru, L. Ungur, *J. Chem. Phys.* **2012**, *137*, 064112; b) M. Böhme, W. Plass, *J. Comput. Chem.* **2018**, *39*, 2697–2712; c) F. Neese, M. Atanasov, G. Bistoni, D. Maganas, S. Ye, *J. Am. Chem. Soc.* **2019**, *141*, 2814–2824; d) M. Böhme, W. Plass, *Chem. Sci.* **2019**, *10*, 9189–9202.

[15] A. E. Ion, E. T. Spielberg, H. Görls, W. Plass, *Inorg. Chim. Acta* **2007**, *360*, 3925–3931.

[16] R. W. G. Wyckoff, *The Analytical Expression of the Results of the Theory of Space-groups*, Carnegie Institution of Washington, Washington, **1922**.

[17] a) A. Burkhardt, A. Buchholz, H. Görls, W. Plass, *Z. Anorg. Allg. Chem.* **2013**, *639*, 2516–2520; b) F.-M. Nie, G. Leibeling, S. Demeshko, S. Dechert, F. Meyer, *Eur. J. Inorg. Chem.* **2007**, 1233–1239.

[18] a) M. Pinsky, D. Avnir, *Inorg. Chem.* **1998**, *37*, 5575–5582; b) H. Zabrodsky, S. Peleg, D. Avnir, *IEEE Trans. Pattern Anal. Mach. Intell.* **1995**, *17*, 1154–1166.

[19] W. Plass, *Z. Anorg. Allg. Chem.* **1997**, *623*, 461–477.

[20] a) A. Roth, A. Buchholz, M. Gärtner, A. Malassa, H. Görls, G. Vaughan, W. Plass, *Z. Anorg. Allg. Chem.* **2007**, *633*, 2009–2018; b) A. Burkhardt, H. Görls, W. Plass, *Carbohydr. Res.* **2008**, *343*, 1266–1277; c) M. Schmidt, H. Görls, W. Plass, *RSC Adv.* **2016**, *6*, 75844–75854.

[21] A. G. Orpen, L. Brammer, F. H. Allen, O. Kennard, D. G. Watson, R. Taylor, *J. Chem. Soc., Dalton Trans.* **1989**, S1–S83.

[22] a) A. P. Ginsberg, R. L. Martin, R. C. Sherwood, *Inorg. Chem.* **1968**, *7*, 932–936; b) A. Escuer, J. Esteban, J. Mayans, M. Font-Bardia, *Eur. J. Inorg. Chem.* **2014**, 5443–5450.

[23] O. Kahn, *Molecular Magnetism*, VCH-Wiley, Weinheim, **1993**.

[24] N. F. Chilton, R. P. Anderson, L. D. Turner, A. Soncini, K. S. Murray, *J. Comput. Chem.* **2013**, *34*, 1164–1175.

[25] A. E. Reed, R. B. Weinstock, F. Weinhold, *J. Chem. Phys.* **1985**, *83*, 735–746.

[26] E. Ruiz, *Chem. Phys. Lett.* **2008**, *460*, 336–338.

[27] E. T. Spielberg, M. Fittipaldi, D. Geibig, D. Gatteschi, W. Plass, *Inorg. Chim. Acta* **2010**, *363*, 4269–4276.

[28] a) E. Ruiz, J. Cano, S. Alvarez, P. Alemany, *J. Comput. Chem.* **1999**, *20*, 1391–1400; b) D. Plaul, D. Geibig, H. Görls, W. Plass, *Polyhedron* **2009**, *28*, 1982–1990.

[29] a) R. Boča, *Coord. Chem. Rev.* **2004**, *248*, 757–815; b) A. Burkhardt, E. T. Spielberg, S. Simon, H. Görls, A. Buchholz, W. Plass, *Chem. Eur. J.* **2009**, *15*, 1261–1271; c) J. Titiš, R. Boča, L. Dlháň, T. Ďurčeková, H. Fuess, R. Ivaniková, V. Mrázová, B. Papánková,

I. Svoboda, *Polyhedron* **2007**, *26*, 1523–1530; d) A. Burkhardt, W. Plass, *Inorg. Chem. Commun.* **2008**, *11*, 303–306.
[30] M. D. Coburn, G. A. Buntain, B. W. Harris, M. A. Hiskey, K.-Y. Lee, D. G. Ott, *J. Heterocycl. Chem.* **1991**, *28*, 2049–2050.
[31] a) COLLECT, Data Collection Software, Nonius B. V., Netherlands, **1998**; b) Z. Otwinowski, W. Minor, *Processing of X-ray Diffraction Data Collected in Oscillation Mode*, in *Methods in Enzymology*, vol. 276, *Macromolecular Crystallography, Part A* (Eds.: C. W. Carter, R. M. Swee), Academic Press, San Diego, USA, **1997**, pp. 307–326.
[32] L. Krause, R. Herbst-Irmer, G. M. Sheldrick, D. Stalke, *J. Appl. Crystallogr.* **2015**, *48*, 3–10.
[33] G. M. Sheldrick, *Acta Crystallogr., Sect. C* **2015**, *71*, 3–8.
[34] TURBOMOLE V7.2 2017, a development of University of Karlsruhe and Forschungszentrum Karlsruhe GmbH, 1989–2007, TURBOMOLE GmbH, since 2007; available from http://www.turbomole.com.
[35] a) E. J. Baerends, D. E. Ellis, P. Ros, *Chem. Phys.* **1973**, *2*, 41–51; b) B. I. Dunlap, J. W. D. Connolly, J. R. Sabin, *J. Chem. Phys.* **1979**, *71*, 3396–3402; c) C. Van Alsenoy, *J. Comput. Chem.* **1988**, *9*, 620–626; d) J. L. Whitten, *J. Chem. Phys.* **1973**, *58*, 4496–4501; e) S. Grimme, J. Antony, S. Ehrlich, H. Krieg, *J. Chem. Phys.* **2010**, *132*, 154104.
[36] a) A. D. Becke, *Phys. Rev. A* **1988**, *38*, 3098–3100; b) J. P. Perdew, *Phys. Rev. B* **1986**, *33*, 8822–8824.
[37] F. Weigend, R. Ahlrichs, *Phys. Chem. Chem. Phys.* **2005**, *7*, 3297–3305.
[38] a) A. D. Becke, *J. Chem. Phys.* **1993**, *98*, 5648–5652; b) C. Lee, W. Yang, R. G. Parr, *Phys. Rev. B* **1988**, *37*, 785–789.
[39] I. Fdez. Galván, M. Vacher, A. Alavi, C. Angeli, F. Aquilante, J. Autschbach, J. J. Bao, S. I. Bokarev, N. A. Bogdanov, R. K. Carlson, L. F. Chibotaru, J. Creutzberg, N. Dattani, M. G. Delcey, S. S. Dong, A. Dreuw, L. Freitag, L. M. Frutos, L. Gagliardi, F. Gendron, A. Giussani, L. González, G. Grell, M. Guo, C. E. Hoyer, M. Johansson, S. Keller, S. Knecht, G. Kovačević, E. Källman, G. Li Manni, M. Lundberg, Y. Ma, S. Mai, J. P. Malhado, P. Å. Malmqvist, P. Marquetand, S. A. Mewes, J. Norell, M. Olivucci, M. Oppel, Q. M. Phung, K. Pierloot, F. Plasser, M. Reiher, A. M. Sand, I. Schapiro, P. Sharma, C. J. Stein, L. K. Sørensen, D. G. Truhlar, M. Ugandi, L. Ungur, A. Valentini, S. Vancoillie, V. Veryazov, O. Weser, T. A. Wesołowski, P.-O. Widmark, S. Wouters, A. Zech, J. P. Zobel, R. Lindh, *J. Chem. Theory Comput.* **2019**, *15*, 5925–5964.
[40] K. Andersson, B. O. Roos, *Chem. Phys. Lett.* **1992**, *191*, 507–514.
[41] a) P.-O. Widmark, P.-A. Malmqvist, B. O. Roos, *Theor. Chim. Acta* **1990**, *77*, 291–306; b) B. O. Roos, R. Lindh, P.-Å. Malmqvist, V. Veryazov, P.-O. Widmark, *J. Phys. Chem. A* **2004**, *108*, 2851–2858; c) B. O. Roos, R. Lindh, P.-Å. Malmqvist, V. Veryazov, P.-O. Widmark, *J. Phys. Chem. A* **2005**, *109*, 6575–6579.
[42] a) L. F. Chibotaru, L. Ungur, C. Aronica, H. Elmoll, G. Pilet, D. Luneau, *J. Am. Chem. Soc.* **2008**, *130*, 12445–12455; b) L. F. Chibotaru, L. Ungur, A. Soncini, *Angew. Chem. Int. Ed.* **2008**, *47*, 4126–4129; c) L. Ungur, W. Van den Heuvel, L. F. Chibotaru, *New J. Chem.* **2009**, *33*, 1224–1230.

Received: November 11, 2019

